Fuel and oxygen harvesting from Martian regolithic brine

Pralay Gayen[a,b,1], Shrihari Sankarasubramanian[a,b,1], and Vijay K. Ramani[a,2]

[a]Center for Solar Energy and Energy Storage, Washington University in St. Louis, St. Louis, MO 63130; and [b]Department of Energy, Environmental and Chemical Engineering, Washington University in St. Louis, St. Louis, MO 63130

Edited by Alexis T. Bell, University of California, Berkeley, CA, and approved November 2, 2020 (received for review May 1, 2020)

NASA's current mandate is to land humans on Mars by 2033. Here, we demonstrate an approach to produce ultrapure H_2 and O_2 from liquid-phase Martian regolithic brine at ∼−36 °C. Utilizing a $Pb_2Ru_2O_{7-\delta}$ pyrochlore O_2-evolution electrocatalyst and a Pt/C H_2-evolution electrocatalyst, we demonstrate a brine electrolyzer with >25× the O_2 production rate of the Mars Oxygen In Situ Resource Utilization Experiment (MOXIE) from NASA's Mars 2020 mission for the same input power under Martian terrestrial conditions. Given the Phoenix lander's observation of an active water cycle on Mars and the extensive presence of perchlorate salts that depress water's freezing point to ∼−60 °C, our approach provides a unique pathway to life-support and fuel production for future human missions to Mars.

electrolyzer | pyrochlore | oxygen evolution reaction | Martian regolith | hypersaline brine

Life-support O_2 and fuel (e.g., H_2) are indispensable for human space exploration. The electrolysis of extraterrestrial liquid water can be a significant concurrent source of H_2 and O_2. NASA's Phoenix lander has found evidence of an active water cycle (1), extensive subsurface ice (2), and the presence of soluble perchlorates (3) on the Martian surface (*SI Appendix*, section S1). Spectral evidence from the Mars Odyssey Gamma Ray Spectrometer points to the existence of large quantities of water-ice in the northern polar region of Mars (4) and the Mars Reconnaissance Orbiter has also found indications of contemporary local flows of liquid regolithic brines shaping Martian geography (5). Martian regolithic brines with dissolved perchlorates (see "Martian regolith composition" in *SI Appendix*, Table S1) can exist in the liquid phase since perchlorates significantly depress the freezing point of water (6). Based on compositional analysis by the wet chemistry instrument on the Phoenix lander, $Mg(ClO_4)_2$ is reported to be a major constituent of the Martian regolith and its concentrated solutions remain in the liquid phase up to ∼−70 °C. This offers a temperature window for the existence of liquid brine on the Martian surface and subsurface as the mean annual terrestrial temperature on Mars is ∼−63 °C (7) with a wide (>100 °C) average diurnal variation (8). The hygroscopic nature of these perchlorates also enables the entrainment of atmospheric water vapor to produce concentrated brine solutions (9). Recently published data obtained by the Mars Advanced Radar for Subsurface and Ionosphere Sounding instrument onboard the Mars Express spacecraft shows that multiple subglacial water bodies presently exist underneath the Martian south pole deposits at Ultimi Scopuli (10).

In support of NASA's mandate to send humans to Mars by 2033 (11), we demonstrate that the electrolysis of these brines at ultralow temperatures is a route to the concurrent production of H_2 as fuel and O_2 for life-support in practical quantities and rates under Martian conditions. NASA has incorporated the Mars Oxygen In-Situ Resource Utilization Experiment (MOXIE) (12) as a part of its Mars 2020 mission (13), as a feasibility study of the electrolysis of CO_2 into CO and O_2 (*SI Appendix*, section S2). As an alternative, we show that regolithic brine electrolysis under Martian conditions will enable the production of ultrapure O_2 for life-support and H_2 for energy production (*SI Appendix*, section S3), with no additional purification requirement for CO removal. The H_2 produced in tandem can serve as a clean-burning fuel with a superior calorific value to CO (*SI Appendix*, section S2). Our electrolyzer system has a 25-fold higher production rate of O_2 when compared to MOXIE while consuming the same amount of power (or, put another way, our system consumes 25× less power than MOXIE for the same O_2 production rate).

Results and Discussion

The Martian atmosphere significantly differs from that of Earth's (14, 15), (*SI Appendix*, Fig. S1) with its predominant constituent being CO_2 [CO_2 reduction has been shown to be unlikely in similar perchlorate electrolytes (9)]. The atmospheric pressure on Mars (6.4 mbar) is also significantly lower than that of Earth (1,013 mbar), but as demonstrated in *SI Appendix*, section 6.2, highly concentrated $Mg(ClO_4)_2$ solutions remain in the liquid phase under Martian temperature and pressure conditions. Considering the above facts, we have conducted experiments with a simulated Martian regolithic brine (SMRB) feed, consisting of 2.8 M $Mg(ClO_4)_2$ solution under CO_2 purging at ultralow temperature (−36 °C), thus simulating the Martian terrestrial environment.

Significance

The active Martian water cycle, i.e., the presence of a shallow water table and soluble perchlorates in the Martian regolith, enables the concurrent production of hydrogen fuel and life-support oxygen on Mars through perchlorate brine electrolysis. Our perchlorate brine electrolyzer operating under simulated Martian surface conditions produces >25× the amount of oxygen produced by the Mars Oxygen In-Situ Resource Utilization Experiment from NASA's Mars 2020 mission for the same input power. This work provides an additional route to help NASA fulfill its mandate to land humans on Mars by 2033. Furthermore, our perchlorate brine electrolyzers are more efficient than state-of-the-art alkaline water electrolyzers under terrestrial conditions, providing a pathway to utilize suboptimal input feeds to produce ultrapure hydrogen and oxygen.

Author contributions: S.S. designed research; P.G. and S.S. performed research; P.G. and S.S. contributed new reagents/analytic tools; P.G., S.S., and V.K.R. analyzed data; and P.G., S.S., and V.K.R. wrote the paper.

Competing interest statement: The authors currently have no financial interests that may be perceived to influence the conclusions presented in this work. The authors are seeking intellectual property protections on aspects of one or more technologies described in this report through the Office of Technology and Management at Washington University in St. Louis (WUSTL).

This article is a PNAS Direct Submission.

Published under the PNAS license.

[1]P.G. and S.S. contributed equally to this work.

[2]To whom correspondence may be addressed. Email: ramani@wustl.edu.

This article contains supporting information online at https://www.pnas.org/lookup/suppl/doi:10.1073/pnas.2008613117/-/DCSupplemental.

First published November 30, 2020.

Downloaded at Palestinian Territory, occupied on December 28, 2021

www.manaraa.com

We have previously demonstrated high-performance alkaline water electrolyzers using $Pb_2Ru_2O_{7-\delta}$ as oxygen evolution reaction (OER) electrocatalysts (*SI Appendix*, section S4) (16). The activity of such electrocatalysts for both oxygen reduction as well as evolution reactions is well established (17). Given this background, we synthesized a $Pb_2Ru_2O_{7-\delta}$ pyrochlore electrocatalyst (see synthesis and material characterization in *SI Appendix*, sections S5.1, S5.2, and S6.1) and examined its OER activity in the SMRB and contrasted it with a RuO_2 benchmark electrocatalyst (*SI Appendix*, section 5.4). Linear sweep voltammograms (LSVs) obtained using thin-film rotating disk electrode (*SI Appendix*, section S5.4) for different catalysts at 21 and −36 °C are depicted in Fig. 1 *A* and *B*, respectively. Initial measurements carried out in O_2-saturated SMRB showed minimal faradaic contributions from the base, glassy carbon (GC) electrode with a small increase in the current at potentials over 1.3 V vs. Ag wire. RuO_2 exhibited OER activity at potentials over 0.9 V vs. Ag wire whereas $Pb_2Ru_2O_{7-\delta}$ was OER-active even at 0.1 V vs. Ag wire. The results confirmed significantly more facile OER kinetics of $Pb_2Ru_2O_{7-\delta}$ when compared to RuO_2 and GC in SMRB. Reports in literature have shown that a Ru-active–site-mediated OER pathway exists for $Pb_2Ru_2O_{7-\delta}$, where the formation of an intermediate involving a higher oxidation state of Ru is recognized as the potential determining step (17, 18). $Pb_2Ru_2O_{7-\delta}$, with higher Ru(V):Ru(IV) ratio, showed higher OER activity as compared to RuO_2 due to the lowered OER activation barrier via the stabilization of the higher oxidation state of the Ru intermediate (*SI Appendix*, section S6.1) (19). The improved OER activity on $Pb_2Ru_2O_{7-\delta}$ is also a function of the surface oxygen vacancies (O-1s X-ray photoelectron spectroscopy (XPS) in *SI Appendix*, Fig. S6) on this electrocatalyst and is further discussed in *SI Appendix*, section S6.3. The higher OER activity for $Pb_2Ru_2O_{7-\delta}$ (higher oxygen vacancy concentration, *SI Appendix*, section S6.1 and S6.3) as compared to benchmark RuO_2 was also attributed to facilitated water dissociation mediated by surface lattice oxygen vacancy quenching and increased bulk conductivity (20, 21). The OER activities for all of the electrodes were also compared upon application of a constant overpotential (200 mV) as depicted in Fig. 1*C* and the relative activity trends were seen to hold across a wide range of temperature from 21 to −36 °C (the corresponding LSVs are depicted in *SI Appendix*, Figs. S6 and S7). Having established the superior OER activity of $Pb_2Ru_2O_{7-\delta}$ in an O_2-saturated SMRB, we examined the OER activity in a CO_2-saturated SMRB more representative of conditions on Mars. The activity and the overpotential were largely unaffected by the shift from O_2 to CO_2-saturated SMRB (within experimental error) as seen in Fig. 1 *A* and *B*. $Pb_2Ru_2O_{7-\delta}$ was also tested across a range of temperatures in CO_2-saturated SMRB (*SI Appendix*, Fig. S7), exhibiting a similar trend as that seen in O_2-saturated SMRB. As detailed in *SI Appendix*, section S6.3, $Pb_2Ru_2O_{7-\delta}$ was found to exhibit greater bifunctional oxygen reduction reaction (ORR)/OER activity as compared to RuO_2 in near-neutral media by applying the Marcus–Hush kinetic formulation to the Tafel analysis of the LSVs (22–24). This provides a pathway for the utilization of the H_2 produced by our Martian electrolyzer in a fuel cell with a $Pb_2Ru_2O_{7-\delta}$ cathode and for the eventual development of a unitized regenerative fuel cell for the use in Mars-like conditions. To identify the limiting reaction in the SMRB electrolyzer, we also examined the hydrogen evolution reaction on Pt/C in CO_2-saturated SMRB over a range of temperatures from 21 to −36 °C (*SI Appendix*, Fig. S11). Given that the ratio of overpotential to current density (i.e., the Tafel slope) is lower for the ORR (94–152 mV/dec) at all of the temperatures compared to the OER (158–173 mV/dec) on $Pb_2Ru_2O_{7-\delta}$ under the same conditions (*SI Appendix*, Fig. S8*C*), it is apparent that the oxygen electrode is the limiting electrode. The ionic conductivity of the electrolyte was also found to exhibit a linear relationship (decrease) with temperature over the entire range from 21 to −36 °C (*SI Appendix*, Fig. S12). The effect of

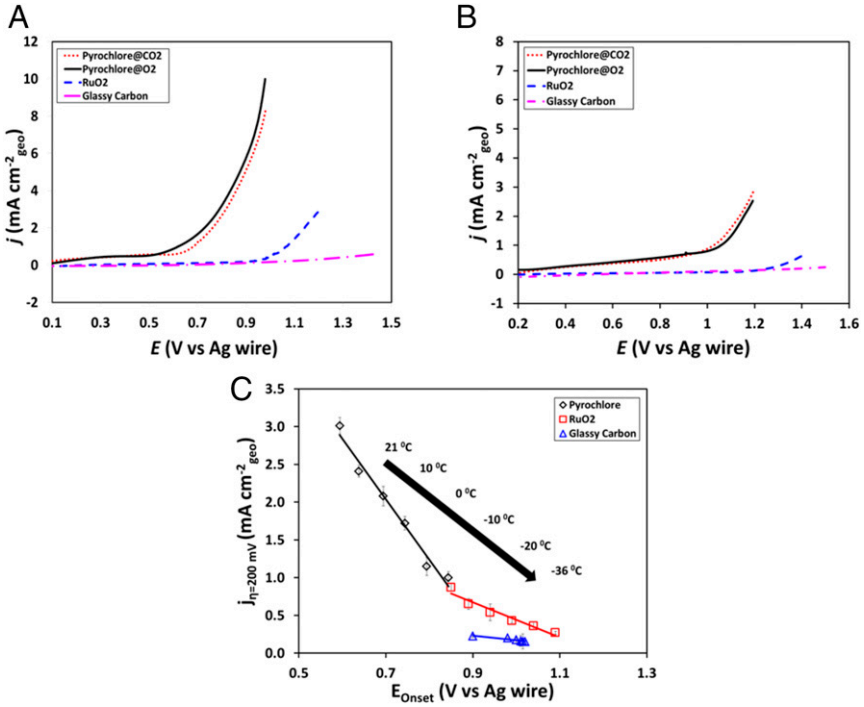

Fig. 1. LSVs of $Pb_2Ru_2O_{7-\delta}$ pyrochlore, RuO_2, and GC in 2.8 M magnesium perchlorate at (*A*) 21 °C and (*B*) −36 °C. (*C*) OER current density at 200-mV overpotential vs. OER onset potential for $Pb_2Ru_2O_{7-\delta}$ pyrochlore, RuO_2, and GC under an O_2-purged environment over a range of temperatures (21 °C [leftmost point] to −36 °C [rightmost point]). E_0 (Ag wire) = 0.44 V vs. SHE at pH = 0, 25 °C and atmospheric pressure.

Downloaded at Palestinian Territory, occupied on December 28, 2021
www.manaraa.com

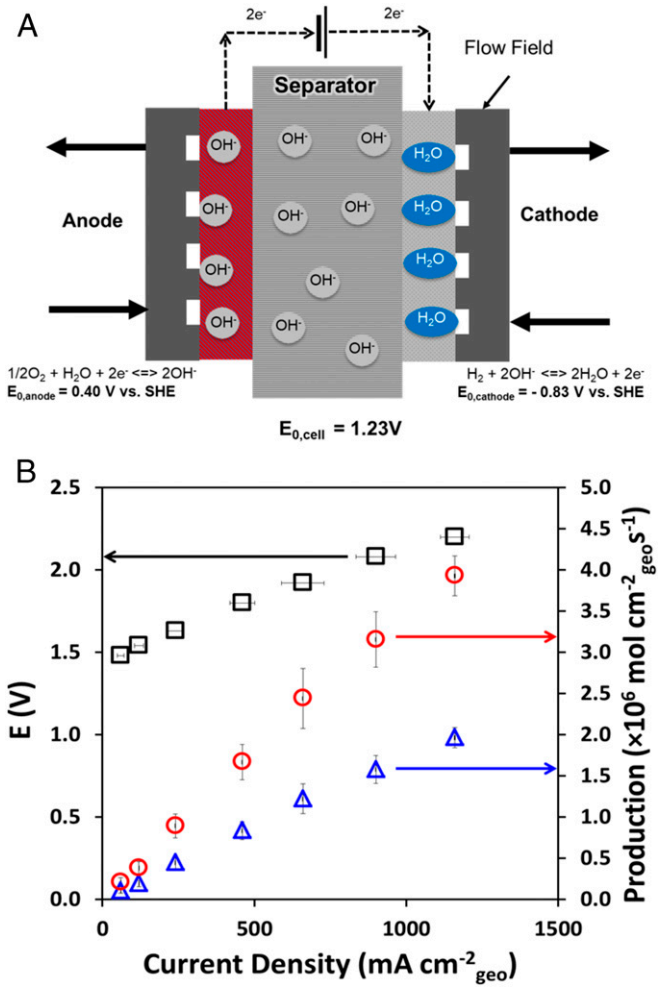

Fig. 2. (*A*) Schematic of the Martian regolithic brine electrolyzer. (*B*) Electrolyzer polarization (E vs. j) and tandem H_2 (red circle)/O_2 (blue triangle) production rate under simulated Martian environment.

change in solution conductivity on OER and ORR activity was considered during the calculation (*iR* drop correction).

Electrolyzers built with $Pb_2Ru_2O_{7-\delta}$ anodes, commercial Fumasep FAA-3–50 anion-exchange membrane (AEM) separators and Pt/C cathodes (Fig. 2*A* and *SI Appendix*, section S5.5) were operated with a 200 mL min^{-1} CO_2-saturated SMRB feed to both the anode and cathode to mitigate water transport/membrane drying issues (25, 26). Anticipated CO_2 poisoning of the AEMs was mitigated by regenerating the AEM using potentiostatic holds at higher potentials (27). Following an initial 30-min potentiostatic hold at 2.5 V, the electrolyzer was polarized in steps between 1.4 and 2.2 V and allowed to relax to a steady electrolyzing current. The resultant polarization (*j-E*) performance was recorded and the corresponding O_2 and H_2 production rates are shown (see *j-E* curve at 21 °C in *SI Appendix*, Fig. S13 and −36 °C in Fig. 2*B*). The produced gases (H_2 and O_2) were kept separated by the AEM in the electrolyzer. They exit through separate tubes, minimizing any cross-over/mixing. No CO_2 reduction was expected based on the measurements by Compton and coworkers (9). For the test in simulated Martian conditions, the feed was constantly purged with CO_2 and the electrolyzer temperature was maintained at −36 °C by employing a carefully calibrated bath of dry ice with an ethylene glycol and ethanol mixture (*SI Appendix*, section S5.3) (28). At both temperatures, the electrolyzer showed excellent performance with peak power densities of 1.23 $W.cm^{-2}$ (1.92 V, −36 °C) and 1.85 $W.cm^{-2}$ (1.85 V, 21 °C), with the decrease in performance in direct correlation to the device temperature being attributed to a combination of lower faradaic currents due to lower reaction rates and increased device resistance due to sluggish ion transport (29). To put the performance in perspective, our previous solid-state alkaline water electrolyzer operating at 50 °C with a $Pb_2Ru_2O_{7-\delta}$ anode achieved a power density of 1.2 $W.cm^{-2}$ at 1.85 V using a deionized (DI) water feed (16). The electrolyzer was found to exhibit a faradaic efficiency of ∼70%, voltage efficiency in the range of 68–100%, and energy efficiency in the range of 36–60% (details in *SI Appendix*, section S6.4) (Fig. 3*A*) and was found to experience an ∼200-mV increase in voltage during a 300-min constant current hold at 400 mA cm^{-2} (Fig. 3*B*). Approximately 80% of the overpotential/activity loss was recovered by holding the electrolyzer at 2.5 V for 30 min. The loss recovery plateaued after 20 min and hence longer potential holds offer diminishing improvements. Previous investigations have attributed similar increases in the electrolyzer resistance to the possible degradation of the commercial AEM binder at the anode as well as the AEM separator (16, 30). Catalyst degradation by the dissolution of Ru from $Pb_2Ru_2O_{7-\delta}$ under electrolyzer operating conditions was also investigated. No such dissolution was observed, suggesting that dissolution, if any, was under the 100-ppb detection limit of our inductive coupled plasma optical emission spectrometer (20). The actual proof-of-concept electrolyzer setup used for the experiment is shown in *SI Appendix*, Fig. S14.

The metrics of the SMRB electrolyzer reported here was compared to existing plans for the generation of O_2 on Mars. MOXIE, developed by the Massachusetts Institute of Technology

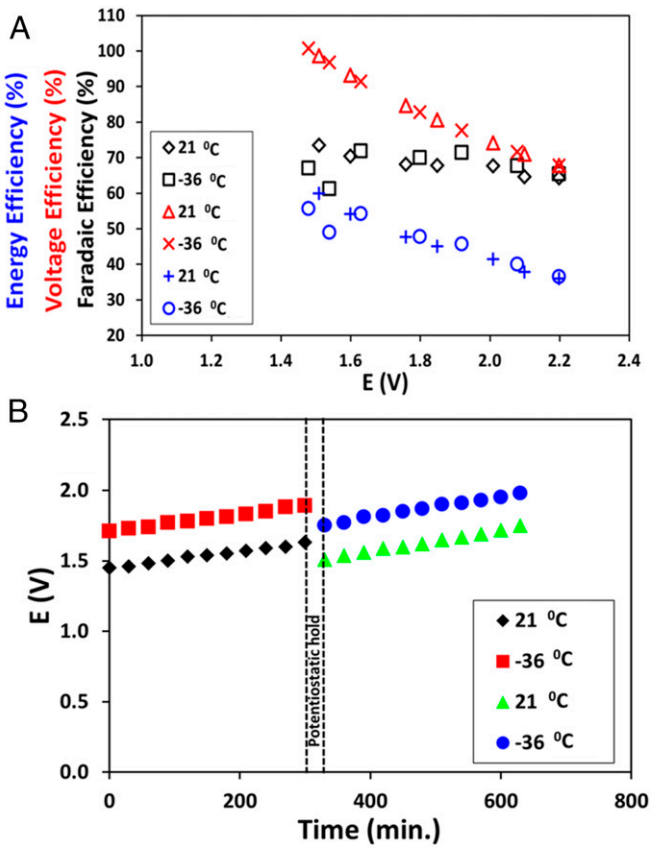

Fig. 3. SMRB electrolyzer (*A*) efficiency and (*B*) stability measurements at 21 and −36 °C. The electrolyzer was held at 2.5 V for 30 min and successfully recovered about 80% of the activity (overpotential) loss.

Downloaded at Palestinian Territory, occupied on December 28, 2021
www.manaraa.com

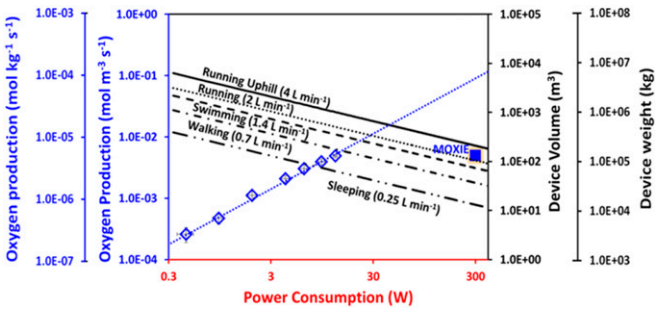

Fig. 4. O_2 production as a function of power consumption (WUSTL electrolyzer and MOXIE), electrolyzer volume, and electrolyzer weight vs. power consumption for different consumption rates.

(MIT) and NASA as a test bed on the Mars 2020 mission, has been designed to produce 10–22 $g{\cdot}h^{-1}$ of O_2 by the electrolysis of CO_2 (31). Utilizing the abundant CO_2 present in the Martian atmosphere, MOXIE produces O_2 and CO, with pure O_2 obtained by subsequent purification. Despite utilizing an abundant and geographically unconstrained feedstock, the production of CO represents a toxic inhalation hazard. Given the differing design philosophies, we have chosen to compare the performance of our electrolyzer with MOXIE purely on the basis of the rate of O_2 production. Fig. 4 depicts O_2 production rate as a function of the electrolyzer power consumption. Further, we have examined the device weight and volume requirements to achieve a given O_2 production rate at rated operating power consumption (see tie lines in Fig. 4). The values of O_2 consumption for various human activities at sea level on Earth were obtained from the US Navy Dive manual (32). To match MOXIE's O_2 production rate (10-22 $g{\cdot}h^{-1}$) our electrolyzer needs to operate at a cell potential of 2.2 V with an electrode area of 28–62 cm^2. A healthy human being requires around 90 $L_{O2}{\cdot}h^{-1}$ and 300 $L_{O2}{\cdot}h^{-1}$ while resting and exercising heavily, respectively. Operating our electrolyzer at 2.2 V, the cell active area required to satisfy these requirements is 375 and 1,235 cm^2, respectively. Our system produces >25× the O_2 as MOXIE while consuming the same amount of power (Fig. 4). Extrapolating to the required production rates for various human activities, our electrolyzer will be smaller in both weight and volume as compared to the current state-of-the-art MOXIE O_2-generator (Fig. 4). Based on these results, we posit that our approach will enable concurrent fuel and oxygen production at viable rates from Martian regolithic brines.

Materials and Methods

The chemicals used and the suppliers along with preparation procedures, characterization methods/conditions are detailed in *SI Appendix*.

The electrochemical measurements were carried out using a three-electrode configuration in a five-neck electrochemical cell with suitable openings for the working, counter, and reference electrodes, the gas purge line inlet, and a gas outlet (Pine Instruments, AKCELL3) (23, 33, 34). The thin-film electrodes for catalyst evaluation were prepared as detailed by us previously (19, 20, 35). The pseudoreference electrode was selected and the low-temperature tests were carried out based on the protocols reported by Compton and coworkers (9). The silver wire pseudoreference electrode used was found to exhibit a potential of 0.44 V vs. standard hydrogen electrode (SHE) at pH = 0, 25 °C and atmospheric pressure. Further details of the effect of temperature, pressure, and pH on the reference electrode potential can be found in prior studies (36, 37). This potential was obtained by calibrating the Ag wire pseudoreference electrode following International Union of Pure and Applied Chemistry recommendations (38, 39) using a well-characterized (40–44) redox probe [$K_4Fe(CN)_6$]. Further details of the reference electrode calibration can be found in our previous studies (22, 24, 33) and in *SI Appendix*, section S5.4. All electrochemical measurements include solution resistance correction (*SI Appendix*, Fig. S13), wherein the resistance was internally measured by the Gamry potentiostat using the current-interrupt method and by measuring the high-frequency resistance (45, 46). The setup for the electrolyzer experiments under simulated Martian conditions is also detailed in *SI Appendix*, section S5.5. The electrolyzer cell separator resistance was measured at different temperatures by electrochemical impedance spectroscopy between the frequencies of 100,000 to 6 Hz with a 10-mV alternating current signal at the open-circuit voltage following recommendations from the literature (47, 48) (*SI Appendix*, Figs. S16 and S17). Given the highly optimized commercial electrolyzer cell design and the highly concentrated electrolyte in use, we attribute the measured high-frequency resistance entirely to the membrane.

Data Availability. All study data are included in the article and *SI Appendix*.

ACKNOWLEDGMENTS. We acknowledge financial support from the McKelvey School of Engineering at Washington University in St. Louis and the Roma B. & Raymond H. Wittcoff Distinguished University Professorship. We acknowledge the Institute of Materials Science and Engineering at Washington University in St. Louis for the use of instruments and staff assistance.

1. J. A. Whiteway *et al.*, Mars water-ice clouds and precipitation. *Science* **325**, 68–70 (2009).
2. P. H. Smith *et al.*, H 2 O at the Phoenix landing site. *Science* **325**, 58–61 (2009).
3. M. H. Hecht *et al.*, Detection of perchlorate and the soluble chemistry of Martian soil at the Phoenix lander site. *Science* **325**, 64–67 (2009).
4. R. Shotwell, Phoenix–The first Mars scout mission. *Acta Astronaut.* **57**, 121–134 (2005).
5. L. Ojha *et al.*, Spectral evidence for hydrated salts in recurring slope lineae on Mars. *Nat. Geosci.* **8**, 829–832 (2015).
6. O. N. Pestova, L. A. Myund, M. K. Khripun, A. V. Prigaro, Physicochemical studies of systems and processes study and thermodynamic analysis of the ZrO 2 SiO 2 system. *Russ. J. Appl. Chem.* **78**, 409–413 (2005).
7. R. Osczevski, Martian windchill in terrestrial terms. *Bull. Am. Meteorol. Soc.* **95**, 533–541 (2014).
8. N. Spanovich *et al.*, Surface and near-surface atmospheric temperatures for the Mars exploration rover landing sites. *Icarus* **180**, 314–320 (2006).
9. J. Elliott, K. Ngamchuea, C. Batchelor-McAuley, R. G. Compton, Martian redox chemistry: Oxygen reduction in low-temperature magnesium perchlorate brines. *J. Phys. Chem. Lett.* **8**, 6171–6175 (2017).
10. S. E. Lauro *et al.*, Multiple subglacial water bodies below the south pole of Mars unveiled by new MARSIS data. *Nat. Astron.*, 10.1038/s41550-020-1200-6 (2020).
11. 115th Congress (2017) National Aeronautics and Space Administration Transition Authorization Act of 2017 (United States of America).
12. NASA, MOXIE - NASA's Mars Exploration Programmars. https://mars.nasa.gov/mars2020/spacecraft/instruments/moxie/. Accessed 8 September 2019.
13. A. Witze, Next stop: Mars. *Nature* **541**, 274–278 (2017).
14. D. R. Williams, Mars Fact Sheet. *NASA Sp Sci Data Coord Arch* (2018). https://nssdc.gsfc.nasa.gov/planetary/factsheet/marsfact.html. Accessed 7 February 2019.
15. R. David, Williams Earth Fact Sheet. *NASA Sp Sci Data Coord Arch:1*. https://nssdc.gsfc.nasa.gov/planetary/factsheet/earthfact.html. Accessed 13 November 2020.
16. J. Parrondo, M. George, C. Capuano, K. E. Ayers, V. Ramani, Pyrochlore electrocatalysts for efficient alkaline water electrolysis. *J. Mater. Chem. A Mater. Energy Sustain.* **3**, 10819–10828 (2015).
17. J. Prakash, D. A. Tryk, E. B. Yeager, Kinetic investigations of oxygen reduction and evolution reactions on lead ruthenate catalysts. *J. Electrochem. Soc.* **146**, 4145 (1999).
18. J. Prakash, D. Tryk, E. Yeager, Electrocatalysis for oxygen electrodes in fuel cells and water electrolyzers for space applications. *J. Power Sources* **29**, 413–422 (1990).
19. P. Gayen, S. Saha, K. Bhattacharyya, V. K. Ramani, Oxidation state and oxygen-vacancy-induced work function controls bifunctional oxygen electrocatalytic activity oxidation state and oxygen-vacancy-induced work function controls bifunctional oxygen electrocatalytic activity. *ACS Catal.* **10**, 7734–7746 (2020).
20. P. Gayen, S. Saha, V. Ramani, Selective seawater splitting using pyrochlore electrocatalyst. *ACS Appl. Energy Mater.* **3**, 3978–3983 (2020).
21. S. Saha, P. Gayen, V. K. Ramani, Facet-dependent chlorine and oxygen evolution selectivity on RuO2: An ab initio atomistic thermodynamic study. *ChemCatChem* **12**, 4922–4929 (2020).
22. S. Sankarasubramanian, J. Seo, F. Mizuno, N. Singh, J. Prakash, Elucidating the oxygen reduction reaction kinetics and the origins of the anomalous Tafel behavior at the lithium-oxygen cell cathode. *J. Phys. Chem. C* **121**, 4789–4798 (2017).
23. S. Sankarasubramanian, J. Seo, F. Mizuno, N. Singh, J. Prakash, Rotating ring-disc electrode investigation of the aprotic superoxide radical electrochemistry on multicrystalline surfaces and correlation with density functional theory modeling: Implications for lithium-air cells. *J. Electrochem. Soc.* **163**, A2377–A2384 (2016).
24. S. Sankarasubramanian, J. Kahky, V. Ramani, Tuning anion solvation energetics enhances potassium-oxygen battery performance. *Proc. Natl. Acad. Sci. U.S.A.* **116**, 14899–14904 (2019).
25. Z. Wang *et al.*, Influence of water transport across microscale bipolar interfaces on the performance of direct borohydride fuel cells. *ACS Appl. Energy Mater.* **3**, 4449–4456 (2020).

Downloaded at Palestinian Territory, occupied on December 28, 2021
www.manaraa.com

26. Z. Wang, S. Sankarasubramanian, V. Ramani, Advances in anion exchange membranes for electrochemical energy conversion. *Curr. Opin. Electrochem.* **12**, 240–245 (2018).
27. J. R. Varcoe *et al*., Anion-exchange membranes in electrochemical energy systems. *Energy Environ. Sci.* **7**, 3135–3191 (2014).
28. C. M. Jensen, D. W. Lee, Dry-ice bath based on ethylene glycol mixtures. *J. Chem. Educ.* **77**, 629 (2009).
29. J. Newman, K. E. Thomas-Alyea, *Electrochemical Systems* (John Wiley and Sons, Hoboken, NJ, ed. 3, 2004).
30. Y. Zhang, J. Parrondo, S. Sankarasubramanian, V. Ramani, Detection of reactive oxygen species in anion exchange membrane fuel cells using in situ fluorescence spectroscopy. *ChemSusChem* **10**, 3056–3062 (2017).
31. F. E. Meyen, M. H. Hecht, J. A. Hoffman, (2015) Thermodynamic model of Mars oxygen ISRU experiment (MOXIE). *Acta Astronaut* **129**, 82–87 (2016).
32. NAVAL SEA SYSTEMS COMMAND U., *U. S. Navy Diving Manual REVISION 7* (2018). https://www.navsea.navy.mil/Portals/103/Documents/SUPSALV/Diving/US%20DIVING%20MANUAL_REV7.pdf?ver=2017-01-11-102354-393 Accessed 13 November 2020.
33. S. Sankarasubramanian, V. Ramani, Dimethyl sulfoxide-based electrolytes for high-current potassium-oxygen batteries. *J. Phys. Chem. C* **122**, 19319–19327 (2018).
34. S. Sankarasubramanian *et al*., Enhancement of oxygen reduction reaction rate by addition of water to an oxidatively stable ionic liquid electrolyte for lithium-air cells. *Electrochem. Commun.* **73**, 55–58 (2016).
35. C. He, G. Wang, J. Parrondo, S. Sankarasubramanian, V. Ramani, Pt/RuO_2-TiO_2 electrocatalysts exhibit excellent hydrogen evolution activity in alkaline media. *J. Electrochem. Soc.* **164**, F1234–F1240 (2017).
36. A. J. Bard, L. R. Faulkner, *Electrochemical Methods: Fundamentals and Applications* (Wiley, ed. 2, 2000).
37. G. Jerkiewicz, Standard and reversible hydrogen electrodes: Theory, design, operation, and applications. *ACS Catal.* **10**, 8409–8417 (2020).
38. J. M. Pingarrón *et al*., Terminology of electrochemical methods of analysis (IUPAC Recommendations 2019). *Pure Appl. Chem.* **92**, 641–694 (2020).
39. G. Gritzner, J. Kuta, Recommendations on reporting electrode potentials in non-aqueous solvents (Recommendations 1983). *Pure Appl. Chem.* **56**, 461–466 (1984).
40. R. C. Murray, P. A. Rock, The determination of the ferrocyanide-ferricyanide standard electrode potential at 25°C in cells without liquid junction using cation-sensitive glass electrodes. *Electrochim. Acta* **13**, 969–975 (1968).
41. G. N. Lewis, L. W. Sargent, The potential of the ferro-ferricyanide electrode. *J. Am. Chem. Soc.* **31**, 355–363 (1909).
42. I. M. Kolthoff, W. J. Tomsicek, The oxidation potential of the system potassium ferrocyanide–potassium ferricyanide at various ionic strengths. *J. Phys. Chem.* **39**, 945–954 (1935).
43. P. A. Rock, The standard oxidation potential of the ferrocyanide-ferricyanide electrode at 25° and the entropy of ferrocyanide ion. *J. Phys. Chem.* **70**, 576–580 (1966).
44. L. M. Peter, W. Dürr, P. Bindra, H. Gerischer, The influence of alkali metal cations on the rate of the Fe(CN)64−/Fe(CN)63− electrode process. *J. Electroanal. Chem. Interfacial Electrochem.* **71**, 31–50 (1976).
45. P. Gayen *et al*., Electrocatalytic reduction of nitrate using Magnéli phase TiO_2 reactive electrochemical membranes doped with Pd-based catalysts. *Environ. Sci. Technol.* **52**, 9370–9379 (2018).
46. P. Gayen, C. Chen, J. T. Abiade, B. P. Chaplin, Electrochemical oxidation of atrazine and clothianidin on Bi-doped SnO_2-Ti_nO_{2n-1} electrocatalytic reactive electrochemical membranes. *Environ. Sci. Technol.* **52**, 12675–12684 (2018).
47. J. Stojadinovic *et al*., Electrochemical characterization of porous diaphragms in development for gas separation. *ECS Electrochem Lett* **1**, F25–F28 (2012).
48. J. Rodríguez *et al*., Simple and precise approach for determination of Ohmic contribution of diaphragms in alkaline water electrolysis. *Membranes (Basel)* **9**, 129 (2019).

Downloaded at Palestinian Territory, occupied on December 28, 2021

www.manaraa.com